Thin-Walled Structures **14** (1992) 59–87

Buckling and Post-buckling Behaviour of Rectangular Plates under Linearly Varying Compression and Shear: Part 1 — Theoretical Analysis

J. Zaraś,[a] J. Rhodes[b] & M. Królak[a]

[a]Institute of Applied Mechanics, Technical University of Łódź, Poland
[b]Division of Mechanics of Materials, University of Strathclyde, UK

(Received 12 June 1990; accepted 10 October 1991)

ABSTRACT

The buckling and post-buckling behaviour of thin, rectangular, simply supported flat plates subjected to end compression which varies linearly in the direction of loading and simultaneously loaded in shear is the subject of this paper. Part 1 presents a theoretical analysis of the problem. In this analysis the Rayleigh–Ritz energy method is utilised, and numerical minimisation of the total potential energy is applied to obtain the magnitude of the parameters of the assumed deflection functions. These are then used to define and describe other post-buckling characteristics of the plate. A simplified imperfection analysis is used to examine certain cases. The wide range of results presented covers many aspects of plate post-buckling behaviour.

NOTATION

a, b	Plate length and breadth, respectively
a_i	Stress function coefficients
B_i, C_i, D_i, H_i	Coefficients used in displacement function u
B_i', C_i', D_i', H_i'	Coefficients used in displacement function v
D	Plate flexural rigidity ($=Et^3/12(1-\nu^2)$)
E	Young's modulus of elasticity
E^*	Apparent modulus of elasticity after buckling

Thin-Walled Structures 0263-8231/92/$05·00© 1992 Elsevier Science Publishers Ltd, England. Printed in Great Britain

E^*/E	Ratio of post-buckling to pre-buckling compressional plate stiffness
f_i	Deflection function coefficient
F	Airy's stress function ($F = F_p + F_c$), such that $\sigma_x = \frac{\partial^2 f}{\partial y^2}$; $\sigma_y = \frac{\partial^2 f}{\partial x^2}$; $\tau_{xy} = \frac{-\partial^2 f}{\partial x \partial y}$
F_p, F_c	Particular integral solution and complementary function solution of the compatibility equation, respectively
i	Natural number index
k_i, l_i, p_i, q_i	Indices used in displacement function u
k_i', l_i', p_i', q_i'	Indices used in displacement function v
m_i, n_i	Integers used in deflection function
$\bar{m}_i, \bar{n}_i$	Integers used in stress function
M_x, M_y, M_{xy}	Moments per unit length
N_x, N_y, N_{xy}	Membrane forces per unit length
Q_x, Q_y	Shearing forces per unit length
t	Plate thickness
u, v	In-plane displacements in x and y directions, respectively ($u = u(xy)$, $v = v(xy)$)
u_o	Plate shortening
U	Work done by external forces
v_o	Shear distortion of the plate
V	Total potential energy
V_b	Strain energy of bending
V_m	Strain energy of mid-plane stresses
V_s	Strain energy ($V_s = V_m + V_b$)
w	Out-of-plane deflections; deflection function ($w = w(x, y)$)
w_e	Experimentally recorded deflection
w_m	Deflection of imperfect plate due to applied load
w_o	Initial plate imperfections
w_p	Perfect plate deflection (also w)
w_t	Total deflection of imperfection plate ($w_t = w_m + w_o$)
x, y, z	Cartesian coordinates
$\varepsilon_x, \varepsilon_y, \gamma_{xy}$	Direct ($\varepsilon_x, \varepsilon_y$) and shear membrane strains (γ_{xy})
$\zeta = \tau/\sigma_1$	Shear stress factor
$\eta = \sigma_2/\sigma_1$	Compression unequality factor
$\lambda = a/b$	Ratio of plate length/breadth
ν	Poisson's ratio (in numerical calculation assumed as 0·3)

$\sigma_{bx}, \sigma_{by}, \tau_{bxy}$ Bending stresses
σ_i Stress intensity calculated using Huber-Hencky-Mises theorem
σ_{prop} Material limit of proportionality
$\sigma_x, \sigma_y, \tau_{xy}$ Membrane stresses
σ_Y Yield stress
σ_1, σ_2, τ External plate loadings
σ_{1cr}, τ_{cr} Critical compressive and shear stresses, respectively

(*) Notation used for non-dimensional values as follows:

$$\sigma^* = \sigma \frac{b^2 t}{\pi^2 D} \qquad w^* = \frac{w}{t}$$

$$\tau^* = \tau \frac{b^2 t}{\pi^2 D} \qquad f_i^* = \frac{f_i}{t}$$

$$u^* = u \frac{b}{\pi^2 t^2} \qquad x^* = \frac{x}{a}; y^* = \frac{y}{b}$$

$$v^* = v \frac{b}{\pi^2 t^2} \qquad V^* = V \frac{4b^2 \lambda}{\pi^2 E t^5}$$

$\nabla^2()$ Laplace operator $\left(\nabla^2() = \dfrac{\partial^2()}{\partial x^2} + \dfrac{\partial^2()}{\partial y^2}\right)$

$\nabla^4()$ Biharmonic operator $\left(\nabla^4() = \dfrac{\partial^4()}{\partial x^4} + 2\dfrac{\partial^2()}{\partial x^2}\dfrac{\partial^2()}{\partial y^2} + \dfrac{\partial^4()}{\partial y^4}\right)$

Other symbols are defined where they first appear.

1 INTRODUCTION

Thin plates are widely used as load-carrying elements in a variety of thin-walled structures, and the buckling and post-buckling of such plates is an important topic. Theoretical investigations of plate buckling and post-buckling behaviour, based on Von Karman's fundamental equations, have been carried out by a large number of researchers over the past five decades. The main results of these investigations have been reviewed in a number of excellent text books.[1-4] A wide variety of different analytical methods, such as the Rayleigh-Ritz method, Galerkin's method, Finite Difference, Finite Element and Finite strip methods have been successfully applied to a wide range of plate problems.

Although the behaviour of plates under uniaxial compression has been the primary focus of attention in the bulk of investigations, there

have also been a large number of examinations of more complex types of loading. In dealing with plate elements of thin-walled structures complex loadings can arise.

The buckling of plates in shear has been examined by various investigators, e.g. Stein and Neff[5] and Porter *et al.*[6] The case of plate elements subject to in-plane bending or, combined bending and axial force has also been the subject of a number of investigations.[7] Two-directional uniform and linearly varying compression of plates has also been subjected to examination by a number of investigators.[8,9] The case of shear which produces varying compression along a plate element, such as occurs in the compression of flange of a beam under varying moment, has been analysed with respect to buckling by, for example, Libove *et al.*,[10] while the post-buckling behaviour has also been analysed.[11] Complex combinations of in-plane compression and shear have been studied by a number of authors, including Protte[12] and Harding *et al.*[13]

The number of publications dealing with plate elements of thin-walled structures is vast and it is not intended here to be in any way exhaustive, but simply to provide a brief background to the examination of plates under complex loadings.

In this paper the objective is to examine the behaviour of a simply supported rectangular plate subjected to end compression which varies linearly in the direction of loading and to shear which is comprised of two components as shown in Fig. 1. This is an approximation to the type of loading which is produced in a compressed flange of an eccentrically loaded box girder as shown in the figure.

2 STATEMENT OF THE PROBLEM

2.1 Basic assumptions and equations

The structure under consideration is a simply supported flat plate of constant thickness loaded by linearly varying compression and shear as shown in Fig. 2.

The normal stress σ_1 and two factors $\eta = \sigma_2/\sigma_1$ and $\zeta = \tau/\sigma_1$ are chosen as loading parameters.

The uniformly distributed additional shear stress τ_o acting along both longitudinal edges results from the equilibrium condition in their x direction.

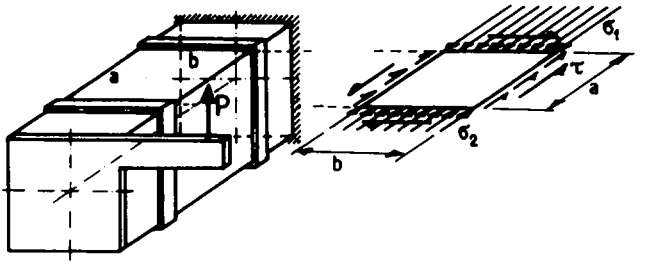

Fig. 1. Plate model as an element of box girder.

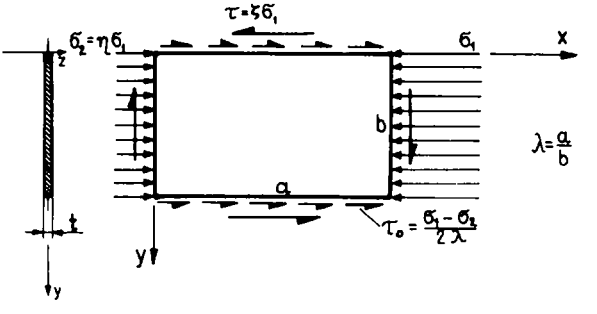

Fig. 2. Loading model of the examined plate.

2.2 Boundary conditions

The assumed simple supports on the boundaries $x = 0, x = a$ are justified by the conditions existing in practice when buckles of the plate create nodal lines perpendicular to direct loading acting in x directions.

Simple support conditions at $y = 0, y = b$, although less accurate for box girder corners, becomes more reliable for the case of a wide flange with longitudinal stiffeners retaining a straight line on the plate-stiffener junction and creating simple support condition along this line.

The boundary conditions therefore are

$$\begin{aligned} &\text{deflection} && w = 0 && \text{at} && x = 0, a;\ y = 0, b \\ &\text{moments} && M_x = M_y = 0 && \text{at} && x = 0, a;\ y = 0, b \\ &\text{hence} && \frac{\partial^2 w}{\partial x^2} = \frac{\partial^2 w}{\partial y^2} = 0 && \text{at} && x = 0, a;\ y = 0, b \end{aligned} \tag{1}$$

2.3 Deflection functions

The buckled shape of the simply supported plate at the instability load is usually assumed as the infinite double sine series

$$w = \sum_{m=1}^{\infty} \sum_{n=1}^{\infty} f_{mn} \sin \frac{m\pi x}{a} \sin \frac{n\pi y}{b} \tag{2}$$

which fulfils the above boundary conditions.

It is known that the accuracy of the approximate solution increases with the number of terms used in the deflection function, but very often it occurs that the first few terms are of significant importance in the final result. So the accuracy of the solution depends on two factors: the ability of the chosen function to represent accurately the actual shape of the plate, and on the number of terms used in the solution to obtain the satisfactory convergence to the actual shape. Against the use of many terms, one has to take into account the greatly increased amount of calculation involved.

The authors decided to limit the deflection function to a five-parameter function

$$w = \sum_{i=1}^{5} f_i \sin \frac{m_i \pi x}{a} \sin \frac{n_i \pi y}{b} \tag{3}$$

where m_i, n_i are the arbitrary chosen number of half-waves in the x and y direction, respectively, related to i; and f_i is the deflection coefficient related to m_i, n_i.

In order to choose the most appropriate terms of eqn (3) suitable for a wide range of loadings represented by σ_1, η, ζ and for different aspect ratios λ, the existing results for simpler load systems were analysed.

After consideration of the buckling of simply supported plates under unequal compression (σ_1, σ_2, τ_o) presented in Refs 10 and 11, and the buckling of plates subjected to pure shear,[5] the indices m_i, n_i of the deflection function (eqn (3)) were assumed as follows:

i	1	2	3	4	5
m_i	1	2	2	2	3
n_i	1	1	2	3	3

(4)

This function was expected to provide satisfactory results for aspect ratios of $0{\cdot}5 \leqslant \lambda \leqslant 2{\cdot}0$ and compression inequality factor $\eta \geqslant 0$ which are frequently encountered in practice. It is obvious, however, that the accuracy of the solution could be improved, especially on the borders of the λ range (0·5, 2·0) and for $\eta < 0$ by including in the deflection function additional terms with m_i, n_i indices of 1,3 and 3,1.

2.4 Airy's stress function F

The stress function F is found in terms of f_i coefficients by solving Von Karman's compatibility equation:

$$\nabla^4 F = E\left[\left(\frac{\partial^2 w}{\partial x \partial y}\right)^2 - \frac{\partial^2 w}{\partial x^2}\frac{\partial^2 w}{\partial y^2}\right] \tag{5}$$

The solution of this differential equation is

$$F = F_p + F_c \tag{6}$$

where F_p is a particular integral solution, and F_c is a complementary function solution.

The particular integral solution F_p, depending on the second derivatives of the deflection function, takes the following form:

$$F_p = E\sum_{i=1}^{30} a_i \cos\bar{m}_i \alpha x \cos\bar{n}_i \beta y \tag{7}$$

where integers $\bar{m}_i$, $\bar{n}_i$ and coefficients a_i related to ith indices are presented in Appendix 1.

As a complementary function solution F_c any solution of the homogeneous biharmonic equation $\nabla^4 F = 0$ can be assumed. In practice, we choose functions which fulfil the external loading boundary conditions. After consideration of the external stresses given in Fig. 2 the F_c function can be expressed as follows:

$$F_c = -\frac{\sigma_1}{2}\left[\eta y^2 + \frac{1-\eta}{a}xy^2 - \frac{(1-\eta)b}{a}xy + 2\zeta xy\right] \tag{8}$$

3 BUCKLING AND POST-BUCKLING ANALYSIS

3.1 General remarks on the solution approach

The theoretical approach used in this chapter employs a Rayleigh–Ritz energy method using the Principal of Minimum Potential Energy. The minimisation of the energy expression with regard to the deflection function coefficients f_i allows for more general analysis at each stage of loading when form and amplitude of the deflection function vector are allowed to sustain changes.

At the onset of buckling, the analysis of the set of simultaneous equations obtained by differentiation of the energy expression with

respect to f_i, can be limited to their linear parts. This is for the reason that at this stage of loading we deal with infinitesimally small values of f_i and can thus reject the higher order terms.

After the initiation of instability the plate can continue to carry increased load, but due to the growth of out-of-plane deflections the stress distribution becomes non-linear and both compressional and bending stiffness of the plate decreases. The semi-numerical solution covering all aspects of plate behaviour is obtained using the results of the energy minimisation procedure.

3.2 Deflection and stress functions

The deflection function employed in the buckling and post-buckling analysis involves the same five terms as given by eqns (3) and (4).

Since the sides of the plate are assumed to be kept straight, the stress function retains its form formulated in the buckling analysis and is given by eqns (6)–(8). This assumption can be related to the general solution for rectangular plates performed by Yamaki[14] who proved that, for the plate with edges kept straight, the stress function does not require the inclusion of the additional complementary function except that part which represents external load. However, the additional hyperbolic terms should be taken into account when the edges are considered free to wave in the plane of the plate.

3.3 Determination of in-plane displacements u, v

The expression for the change in potential energy of the applied external loadings requires the knowledge of in-plane displacements u and v on the edges of the plate. The full 'displacement field $u(xy)$, $v(xy)$' can be derived using the basic expressions for middle plane strains $\varepsilon_x, \varepsilon_y, \gamma_{xy}$ of the buckled plate.

$$\varepsilon_x = \frac{1}{E}(\sigma_x - \nu\sigma_y) = \frac{\partial u}{\partial x} + \frac{1}{2}\left(\frac{\partial w}{\partial x}\right)^2 \tag{9}$$

$$\varepsilon_y = \frac{1}{E}(\sigma_y - \nu\sigma_x) = \frac{\partial v}{\partial y} + \frac{1}{2}\left(\frac{\partial w}{\partial y}\right)^2 \tag{10}$$

$$\gamma_{xy} = \frac{2(1+\nu)}{E}\tau_{xy} = \frac{\partial u}{\partial y} + \frac{\partial v}{\partial x} + \frac{\partial w}{\partial x}\frac{\partial w}{\partial y} \tag{11}$$

By suitable rearrangements of the eqns (9)–(11) in which the stresses are substituted by stress function F, the expressions for first derivatives $\partial u/\partial x$, $\partial u/\partial y$, $\partial v/\partial x$, $\partial v/\partial y$ can be found. These, after integration,

permitted determination of the displacements $u(xy)$ and $v(xy)$. While calculating the integration constants it is required to introduce the condition against the plate 'body movement' which can be accomplished by inhibition of three displacement components of any two points 'P1' and 'P2' as shown in Fig. 3.

The final expressions for the displacements $u(xy)$ and $v(xy)$ are given in Appendix 2. The typical form of the displacements of the plate edges is shown in Fig. 4.

It should be pointed out that the difference between σ_1 and σ_2 causes the compressed edges to become parabolas of identical shape given by expression

$$u_p = \frac{\sigma_1}{2E}(2 + \nu)(1 - \eta)\left(\frac{y^2}{a} - \frac{y}{\lambda}\right) \tag{12}$$

Therefore, each fibre parallel to the x axis is shortened by this same amount which is equal to the total plate shortening u_o defined as

$$u_o = -[u(xy)_{x=a} - u(xy)_{x=0}] \tag{13}$$

The total distortion v_o has been defined as the difference between

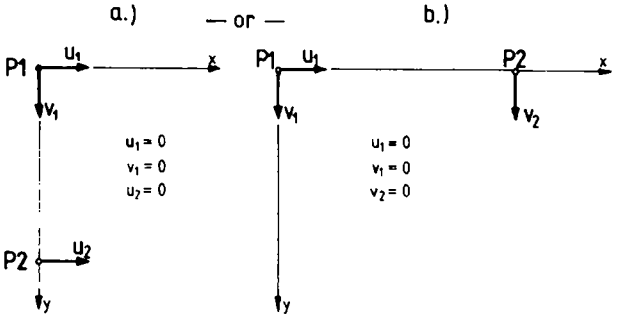

Fig. 3. Conditions for inhibition of the 'body movement' of the plate.

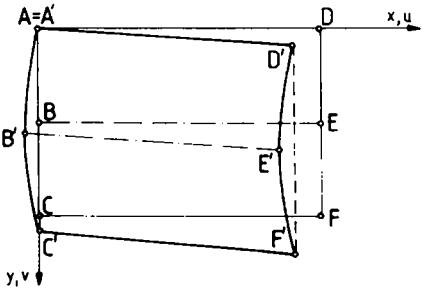

Fig. 4. Edge displacements of the plate.

displacements of the central points 'E' and 'B' in the y direction (see Fig. 4).

$$v_o = v(xy)_{x=a,y=b/2} - v(xy)_{x=0,y=b/2} \tag{14}$$

u_o and v_o are given in full in Appendix 2.

3.4 Determination of energy — V

The change in potential energy, V, is represented by eqn (15) involving the strain energy ($V_m + V_b$) and work done by the external loadings (U):

$$V = V_m + V_b - U \tag{15}$$

The strain energy of mid-surface forces is as follows:

$$V_m = \frac{t}{2E}\int_0^a \int_0^b \left(\frac{\partial^2 F}{\partial x^2} + \frac{\partial^2 F}{\partial y^2}\right)^2 - 2(1+\nu)\left[\frac{\partial^2 F}{\partial x^2}\frac{\partial^2 F}{\partial y^2} - \left(\frac{\partial^2 F}{\partial x \partial y}\right)^2\right]dx\,dy \tag{16}$$

The strain energy due to bending takes the form

$$V_b = \frac{1}{2}D\int_0^a \int_0^b \left(\frac{\partial^2 w}{\partial x^2} + \frac{\partial^2 w}{\partial y^2}\right)^2 - 2(1-\nu)\left[\frac{\partial^2 w}{\partial x^2}\frac{\partial^2 w}{\partial y^2} - \left(\frac{\partial^2 w}{\partial x \partial y}\right)^2\right]dx\,dy \tag{17}$$

By integration of all external edge-force edge-displacement products the change in the potential of external forces, or the work due to external forces is obtained:

$$U = \left[t\int_0^b (p_x u + sv)dy\right]_{x=0}^{x=a} + \left[t\int_0^a (p_y v + su)dx\right]_{y=0}^{y=b} \tag{18}$$

where the external stresses on the plate edges are

$$p_x = \frac{\partial^2 F_c}{\partial y^2};\quad p_y = \frac{\partial^2 F_c}{\partial x^2};\quad s = -\frac{\partial^2 F_c}{dx\,dy} \tag{19}$$

After substituting the required functions F and w into eqns (16) and (17) and edge displacements–stress products into eqn (18) and performing all the integrations prescribed the final expression for the change in potential energy V is obtained.

$$V = -t\frac{\sigma_1^2 b^2}{6E}\lambda\left[(\eta^2+\eta+1)+\frac{(1+\nu)(1-\eta)^2}{2\lambda^2}\right]-t\frac{\sigma^2 b^2}{E}\lambda(1+\nu)\zeta^2$$
$$-\frac{tE\pi^4}{4b^2\lambda}\Big[\, f_1^2\frac{1}{2}W_{11}+f_2^2\frac{1}{2}W_{22}+f_3^2\frac{1}{2}W_{33}+f_4^2 W_{44}+f_5^2\frac{1}{2}W_{55}$$
$$+f_1 f_2 W_{12}+f_1 f_3 W_{13}+f_1 f_4 W_{14}+f_2 f_5 W_{25}+f_3 f_5 W_{35}$$
$$+f_4 f_5 W_{45}+f_1 f_2 f_4 f_5 W_{1(245)}+f_1^2 f_2 f_4\frac{1}{2}W_{1(124)}+f_1 f_2^2 f_5 W_{1(225)}$$
$$+f_2 f_3^2 f_4 W_{2(334)}+f_1^2 f_2^2\frac{1}{2}W_{1(122)}+f_1^2 f_3^2\frac{1}{2}W_{1(133)}+f_1^2 f_4^2\frac{1}{2}W_{1(144)}$$
$$+f_1^2 f_5^2\frac{1}{2}W_{1(155)}+f_2^2 f_3^2\frac{1}{2}W_{2(233)}+f_2^2 f_4^2\frac{1}{2}W_{2(244)}+f_2^2 f_5^2\frac{1}{2}W_{2(255)}$$
$$+f_3^2 f_4^2\frac{1}{2}W_{3(344)}+f_3^2 f_5^2\frac{1}{2}W_{3(355)}+f_4^2 f_5^2\frac{1}{2}W_{4(455)}+f_2^3 f_4\frac{1}{3}W_{2(224)}$$
$$+f_1^4\frac{1}{4}W_{1(111)}+f_2^4\frac{1}{4}W_{2(222)}+f_3^4\frac{1}{4}W_{3(333)}+f_4^4\frac{1}{4}W_{4(444)}$$
$$+f_5^4\frac{1}{4}W_{5(555)}\Big] \qquad (20)$$

where the coefficients W_{ij} and $W_{i(jkl)}$ are given in Appendix 3.

3.5 Buckling analysis and its numerical results

After differentiation of the energy expression V (eqn (20)) against the deflection function coefficients f_i, the following set of five simultaneous cubic equations is obtained.

$$f_1 W_{11}+f_2 W_{12}+f_3 W_{13}+f_4 W_{14}+f_5 W_{15}+f_1^3 W_{1(111)}+f_1 f_2^2 W_{1(122)}$$
$$+f_1 f_3^2 W_{1(133)}+f_1 f_4^2 W_{1(144)}+f_1 f_5^2 W_{1(155)}+f_1 f_2 f_4 W_{1(124)}$$
$$+f_2 f_4 f_5 W_{1(245)}+f_2^2 f_5 W_{1(225)} = 0 \qquad (21a)$$
$$f_1 W_{21}+f_2 W_{22}+f_3 W_{23}+f_4 W_{24}+f_5 W_{25}+f_1^2 f_2 W_{2(112)}+f_1^2 f_4 W_{2(114)}$$
$$+f_1 f_2 f_5 W_{2(125)}+f_1 f_4 f_5 W_{2(145)}+f_2^3 W_{2(222)}+f_2^2 f_4 W_{2(224)}$$
$$+f_2 f_3^2 W_{2(233)}+f_2 f_4^2 W_{2(244)}+f_2 f_5^2 W_{2(255)}+f_3^2 f_4 W_{2(334)} = 0 \qquad (21b)$$
$$f_1 W_{31}+f_2 W_{32}+f_3 W_{33}+f_4 W_{34}+f_5 W_{35}+f_1^2 f_3 W_{3(113)}+f_2^2 f_3 W_{3(223)}$$
$$+f_2 f_3 f_4 W_{3(234)}+f_3^3 W_{3(333)}+f_3 f_4^2 W_{3(344)}+f_3 f_5^2 W_{3(355)} = 0 \qquad (21c)$$

$$f_1 W_{41} + f_2 W_{42} + f_3 W_{43} + f_4 W_{44} + f_5 W_{45} + f_1^2 f_2 W_{4(112)} + f_1^2 f_4 W_{4(114)} + f_1 f_2 f_5 W_{4(125)} + f_2^3 W_{4(222)} + f_2^2 f_4 W_{4(224)} + f_2 f_3^2 W_{4(233)} + f_3^2 f_4 W_{4(334)} + f_4^3 W_{4(444)} + f_4 f_5^2 W_{4(455)} = 0 \tag{21d}$$

$$f_1 W_{51} + f_2 W_{52} + f_3 W_{53} + f_4 W_{54} + f_5 W_{55} + f_1^2 f_5 W_{5(115)} + f_1 f_2^2 W_{5(122)} + f_1 f_2 f_4 W_{5(124)} + f_2^2 f_5 W_{5(225)} + f_3^2 f_5 W_{5(335)} + f_4^2 f_5 W_{5(445)} + f_5^3 W_{5(555)} = 0 \tag{21e}$$

It is worthwhile to mention that in this case the above expressions can also be obtained from the Galerkin method.

While considering the instability initiation the eigenvector components can be regarded as very small and therefore for the buckling problem eqns (21a–e) can be restricted to their linear parts. The set of linear equations involved in the buckling problem can then be expressed as follows:

$$\begin{bmatrix} W_{11} & \dots & W_{15} \\ . & \dots & . \\ W_{51} & \dots & W_{55} \end{bmatrix} \begin{bmatrix} f_1 \\ . \\ f_5 \end{bmatrix} = 0 \tag{22}$$

The critical stresses are obtained as a non-trivial solution of eqn (22), which must fulfil the zero condition for the determinant $|W|$ of matrix $[W]$

$$Det\,|W| = 0 \tag{23}$$

The numerical procedure was performed in non-dimensional form.

The critical state of the plate is represented by the lowest pair of stresses σ_{1cr}^* and τ_{cr}^* for given discrete values of factors λ and η. The plates examined numerically covered the range of aspect rations $\lambda = a/b$ of $0{\cdot}5 \leqslant \lambda \leqslant 2{\cdot}0$ and compression unequality factors from the range $0 \leqslant \eta \leqslant 1{\cdot}0$. The results of numerical calculations are presented in Figs 5–8.

The graphs presented in Fig. 5 show the non-dimensional buckling load of the plate under unidirectional varying compression, expressed in terms of aspect ratio λ for three arbitrarily chosen values of unequality factor η. The results are compared with those obtained by Libove *et al.*[10] Figure 6 shows the buckling coefficients τ_{cr}^* for pure shear in terms of aspect ratio λ and compared with the results presented by others.

The curves presented in Fig. 7 show the average non-dimensional critical stress $\sigma_{avcr}^* = \sigma_{1cr}^*(1 + \eta)/2$ against the aspect ratio λ. It is

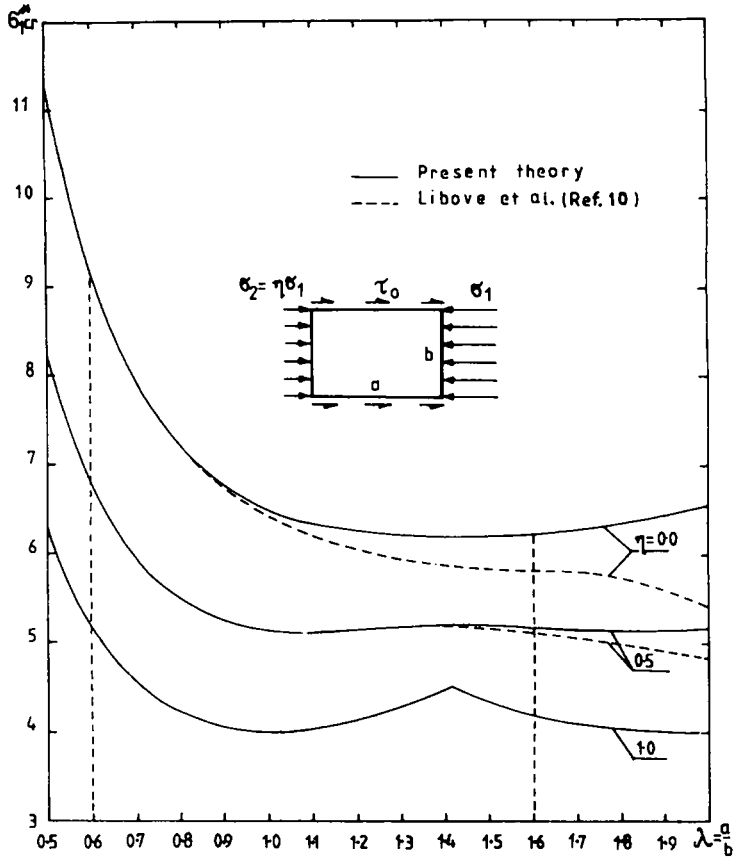

Fig. 5. Critical loading σ^*_{1cr} versus length to width ratio $\lambda = a/b$.

noticeable from the results presented that increasing unqeuality between σ_1^* and σ_2^* (i.e. $\eta \to 0$) causes a decrease in the average buckling stress.

In Fig. 8 the samples of buckling coefficients for complex loadings involving compression and shear are shown. The cases when $\lambda \geqslant 1$ and $\eta = 1{\cdot}0$ are compared with the results presented by Stowell and Schwartz,[15] who for these cases suggested the following approximate relationship for critical stresses:

$$\frac{\sigma_x}{(\sigma_x)_{cr}} + \left[\frac{\tau_{xy}}{(\tau_{xy})_{cr}}\right]^2 = 1 \tag{24}$$

The inaccuracies of the present results concerning critical loadings should not noticeably exceed the limit of 5% which is acceptable from a practical point of view, provided that the parameters of plate geometry and loading factors are limited to the following ranges: $0{\cdot}6 \leqslant \lambda \leqslant 1{\cdot}6$, $0 \leqslant \eta \leqslant 1{\cdot}0$, $0 \leqslant \zeta \leqslant 1{\cdot}0$.

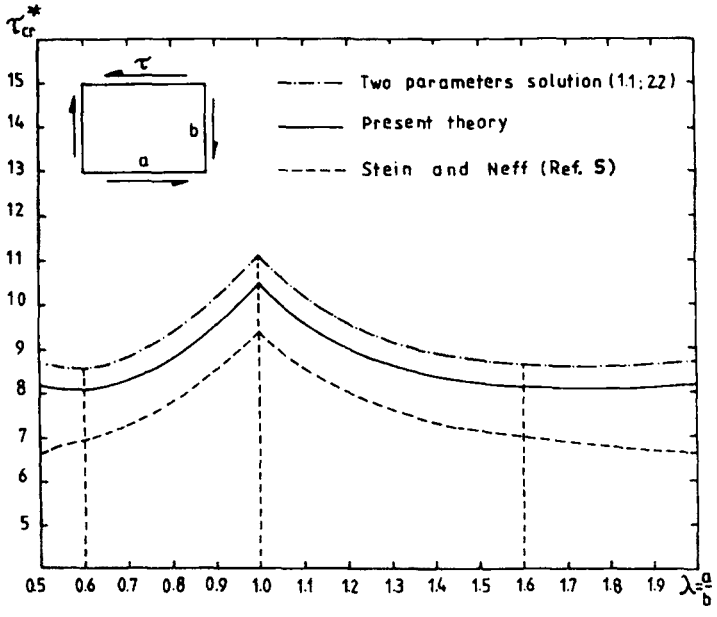

Fig. 6. Critical shear τ_{cr}^* versus length to width ratio $\lambda = a/b$.

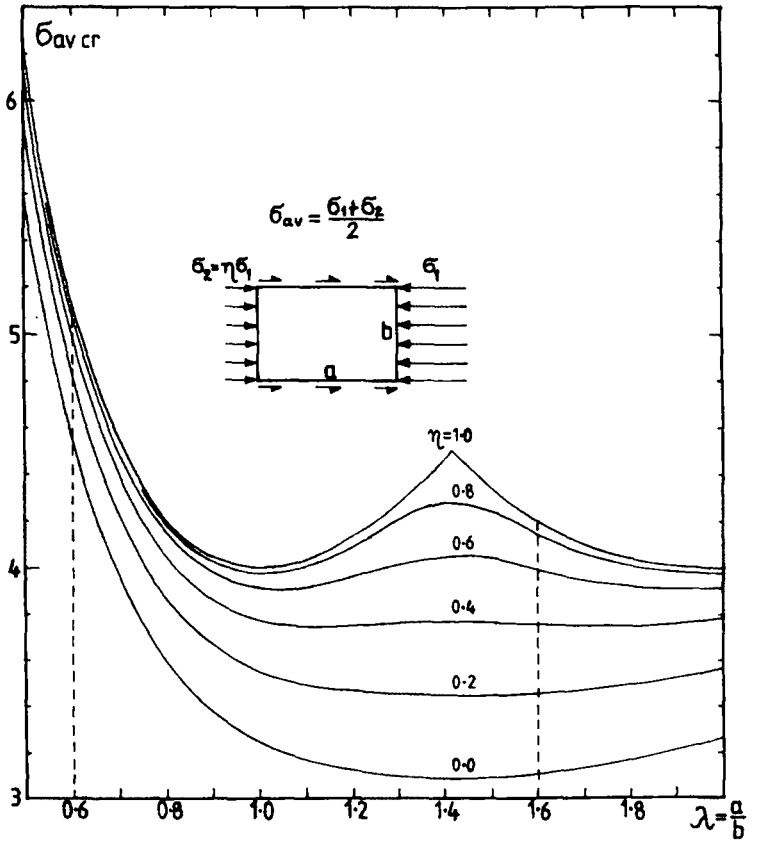

Fig. 7. Critical average stress σ_{avcr}^* versus length to width ratio $\lambda = a/b$.

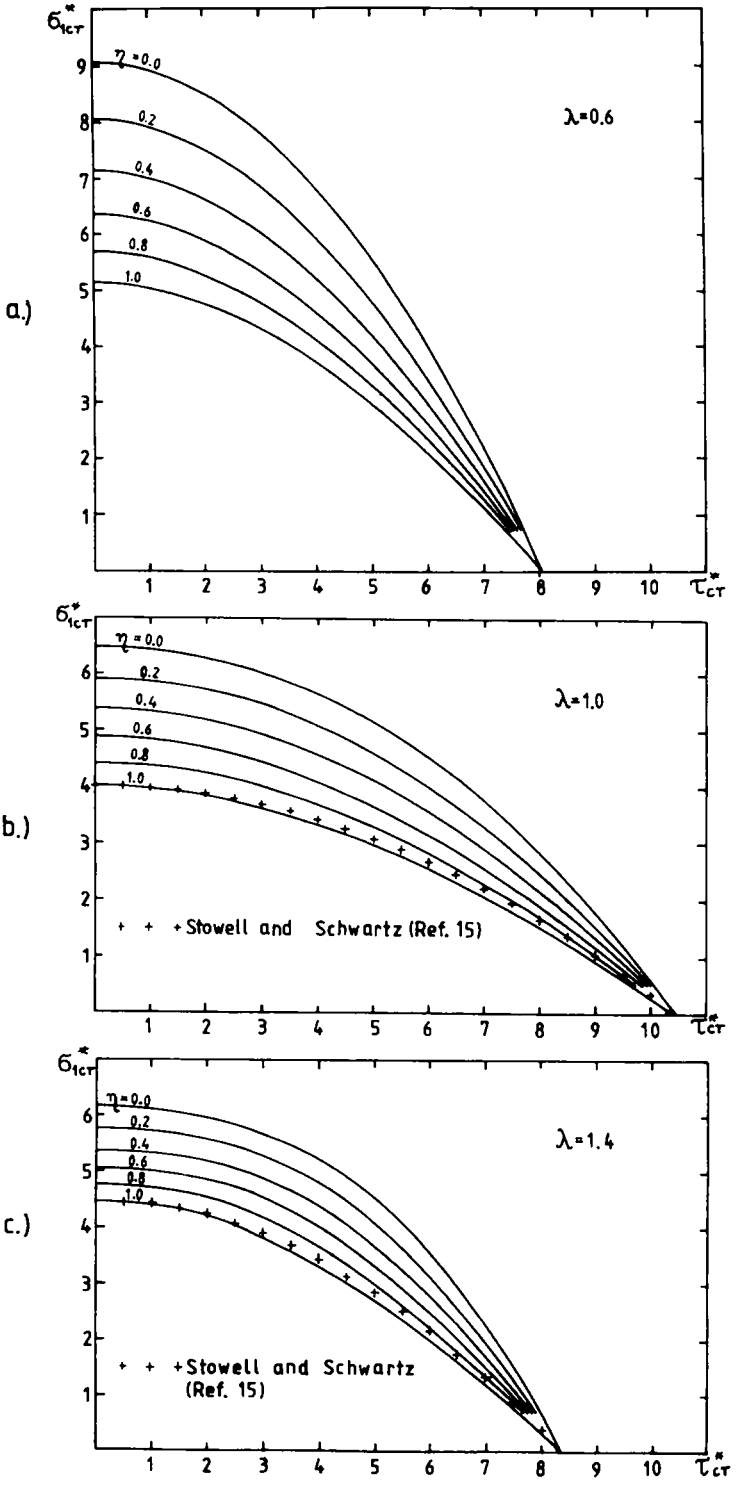

Fig. 8. Critical compression σ_1^* versus critical shear τ_{cr}^*.

3.6 Stresses

The expressions for all stress components at any point of the plate can be determined using stress function, F, and deflection, w.

Membrane stress components are

$$\sigma_x = \frac{\partial^2 F}{\partial y^2}; \quad \sigma_y = \frac{\partial^2 F}{\partial x^2}; \quad \tau_{xy} = -\frac{\partial^2 F}{\partial x \partial y} \tag{25}$$

Bending stress components are given by

$$\begin{aligned} \sigma_{bx} &= -\frac{Ez}{1-\nu^2}\left(\frac{\partial^2 w}{\partial x^2} + \nu \frac{\partial^2 w}{\partial y^2}\right) \\ \sigma_{by} &= -\frac{Ez}{1-\nu^2}\left(\frac{\partial^2 w}{\partial y^2} + \nu \frac{\partial^2 w}{\partial x^2}\right) \\ \tau_{bxy} &= -\frac{Ez}{1+\nu}\frac{\partial^2 w}{\partial x \partial y} \end{aligned} \tag{26}$$

The stress intensity at any point of the plate can be calculated using the Huber-Hencky-Mises theorem:

$$\sigma_i = \sqrt{(\sigma_x + \sigma_{bx})^2 + (\sigma_y + \sigma_{by})^2 - (\sigma_x + \sigma_{bx})(\sigma_y + \sigma_{by}) + 3(\tau_{xy} - \tau_{bxy})^2} \tag{27}$$

3.7 Numerical results in post-buckling range

3.7.1 Basic characteristics of the plate behaviour

The numerical calculations were carried out employing non-dimensional forms of all expressions and arguments involved. Basic characteristics of plate post-buckling behaviour are represented by the overall stress intensity σ_{oi}^*, maximum deflection $w_{\max}^*$, plate shortening u_o^* and plate distortion v_o^* all expressed in terms of loadings σ_1^*.

The overall stress intensity σ_{oi}^* was taken as the maximum value from all σ_i^* calculated for top and bottom surfaces of the plate.

A plate, whose dimensions and type of loading are known, i.e. a plate in which parameters λ, η, ζ are fixed, was regarded as one calculation variant. A solution of a single variant at particular loading level σ_1^* is accomplished when the deflection parameters f_i^* corresponding to the minimum of the energy expression V^* are found. These parameters permitted the calculation of all stress components and stress intensity on the top and bottom surfaces in the discrete points x^*, y^* of the net with the mesh of $\Delta x^* = \Delta y^* = 0{\cdot}1$. In the same points the deflection w^* was

also evaluated. The maximum deflection w^*_{max} has been determined by applying a minimisation procedure to the deflection function. At the same time the shortening u^*_o and the shear distortion v^*_o were calculated. This completed a set of data obtained at one particular loading σ^*_1. The energy minimisation procedure was based on Powell's method. The increase of plate load σ^*_1 was continued numerically and the calculation of one variant was finished when the overall stress intensity σ^*_{oi} reached the non-dimensional limit of proportionality σ^*_{prop}.

Typical results of theoretical investigations are shown in Figs 9–13. A feature which characterises most of the results obtained is a visible division of the curves into two separate sets. The first set of curves, usually for lower shear stress factors $\zeta(\zeta = 0{\cdot}0, 0{\cdot}2, 0{\cdot}4)$, is tightly spaced and presents a compressive type of plate behaviour. The second set of curves is of interactive character, when the compression and shear contribute equally to the post-buckling behaviour of the plate. This division does not occur between $\zeta = 0{\cdot}4$ and $\zeta = 0{\cdot}6$ since it is influenced by the aspect ratio λ and the factor η. The curves σ^*_{oi} versus σ^*_1 in Fig. 9 allow quick assessment of the plate carrying capacity corresponding to the limit of proportionality. The maximum deflections (e.g. Fig. 10) in the majority of cases examined showed typical parabolic character. The changes of the slope of the curves u^*_o versus σ^*_1 (e.g. those in Fig. 11) imply gradual change of the post-buckled form of the mid-surface of the plate. The distinctive difference between compression and compression–shear type behaviour becomes even more evident when the shear distortion v^*_o versus σ^*_1 is considered. By comparing Figs 11 and 12 it becomes clear

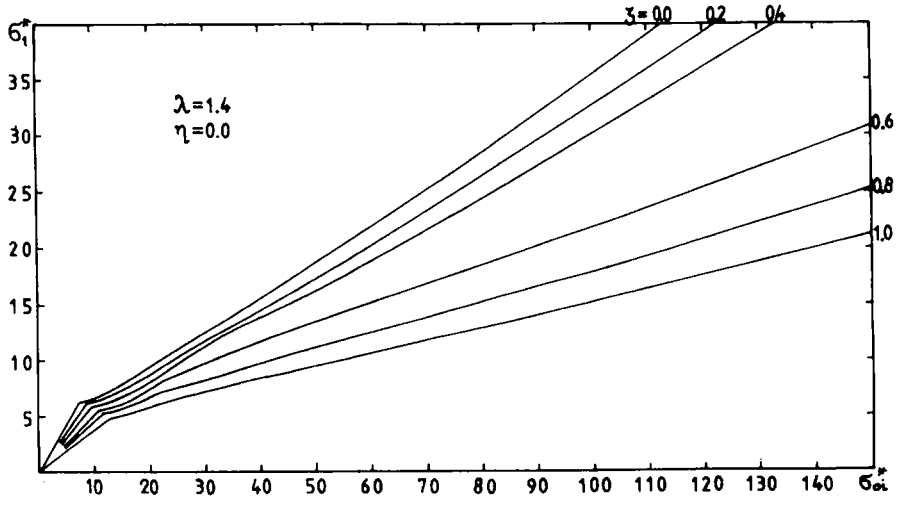

Fig. 9. Overall stress intensity σ^*_{oi} versus loading parameter σ^*_1.

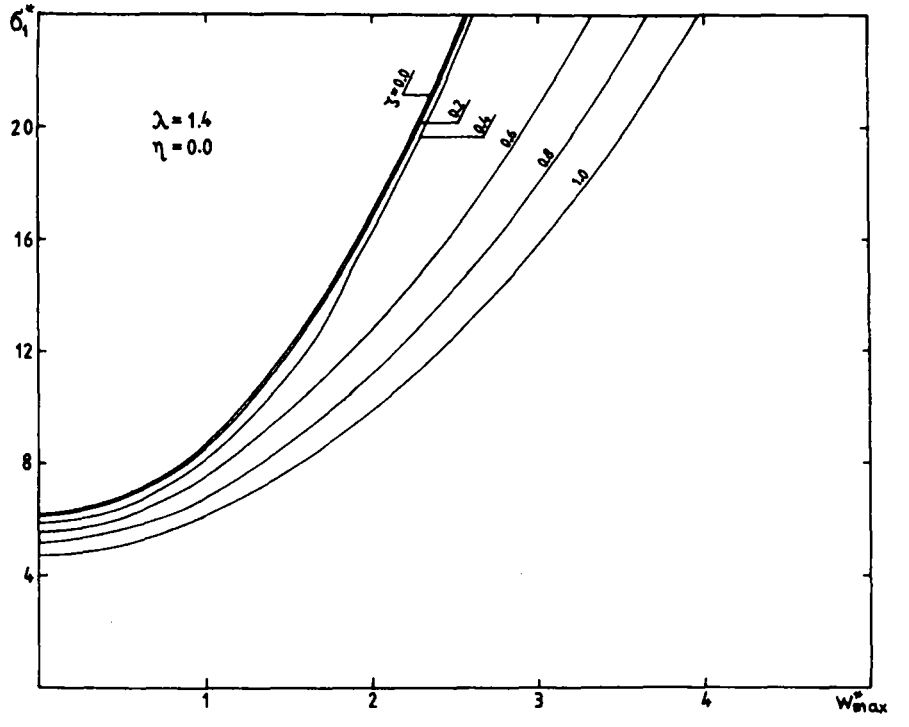

Fig. 10. Maximal deflection w^*_{max} versus loading parameter σ^*_1.

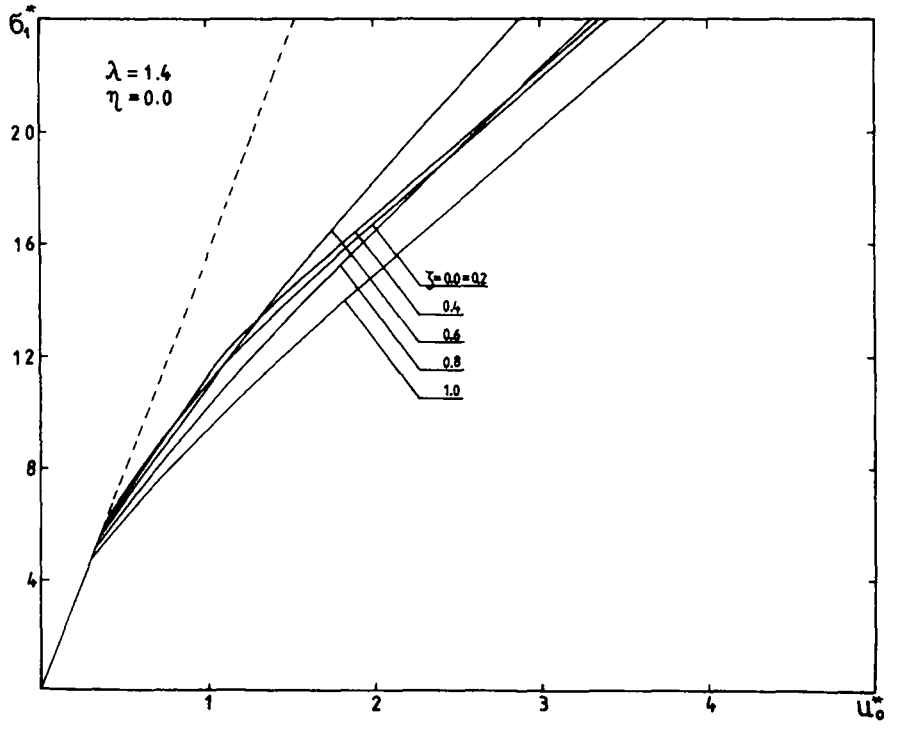

Fig. 11. Plate shortening u^*_o versus loading parameter σ^*_1.

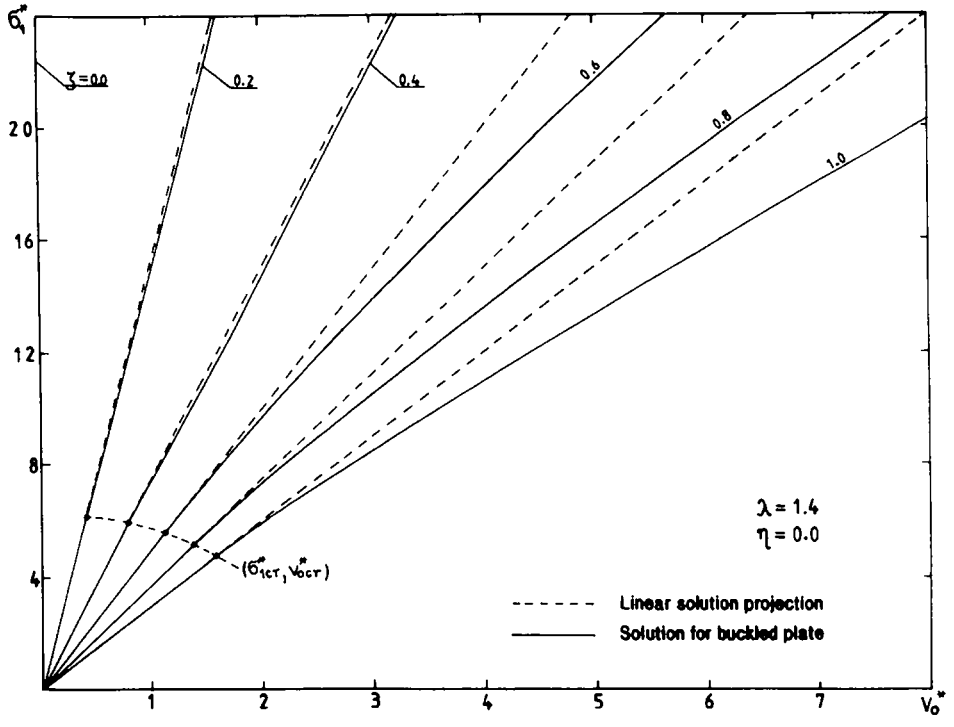

Fig. 12. Shear distortion v_o^* versus loading parameter σ_1^*.

that the 'surprising' increase of the compression stiffness of the curves at $\zeta = 0{\cdot}6, 0{\cdot}8, 1{\cdot}0$ compared to those at $\zeta = 0{\cdot}0, 0{\cdot}2, 0{\cdot}4$ is taking place at the expense of a substantial decrease of shear stiffness. An interesting point is that in certain cases the results obtained imply a snap-through change of the plate shape.

3.7.2 Post-buckling to pre-buckling stiffness of the plate E*/E

The ratio of post-buckling compressional stiffness to that before buckling is given in Ref. 16 by the ratio of E^*/E in which E^* denotes the apparent modulus of elasticity after buckling. The approximate expression for E^*/E can be determined from the discrete values of the u_o^* versus σ_1^* curve using the geometrical relations shown in Fig. 13.

The value of E^*/E given by the expression

$$\frac{E^*}{E} = \frac{\Delta\sigma_1^*/\Delta u_o^*}{\sigma^*{}_{1cr}/u_{ocr}^*} \tag{28}$$

is related to the point $\sigma_1^*(E^*/E) = \sigma_1^* + \Delta\sigma_1^*/2$

In Fig. 14 typical examples of the ratio E^*/E for two cases of shear stress factors $\zeta = 0{\cdot}0$ and $1{\cdot}0$ are presented. The value of compressional

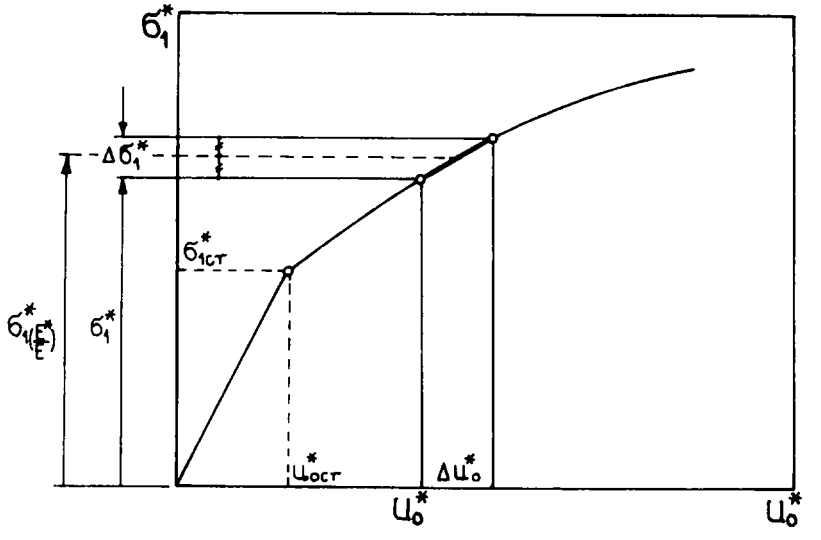

Fig. 13. Model for evaluation of post-buckling stiffness E^*/E.

stiffness of the plate drops sharply at the instant of buckling and in the post-buckling range decreases gradually with the increase in loading.

4 SIMPLIFIED ANALYSIS OF IMPERFECT PLATE

The results presented so far are obtained for perfectly flat plates. Rigourous theoretical analysis of the imperfect plates corresponding to the cases examined would require complicated mathematical derivations and prolonged numerical calculations.

In many practical situations, however, there is a need to determine the behaviour of the plate with initial deformations in a simplified manner which produces a reasonably accurate solution without involving much additional calculations. It has been proved by Williams and Walker[17] and Rhodes and Harvey[18] that the behaviour of the compressed imperfect plate with various boundary restraints can be formulated simply by employing the results of perfect plate solution and assumption that the imperfections were of the same general form as the buckling mode. The expression for the load-deflection relationship of the plate with moderate initial imperfections given by Williams and Walker is

$$P^* = P^*_{cr}\left(1 - \frac{w_o^*}{w_t^*}\right) + \frac{P^*_{cr}}{A^2}(w_t^{*2} - w_o^{*2}) \tag{29}$$

where P^* is the actual load corresponding to σ_1^*, P^*_{cr} is the critical load, and A is a constant dependent on the boundary conditions.

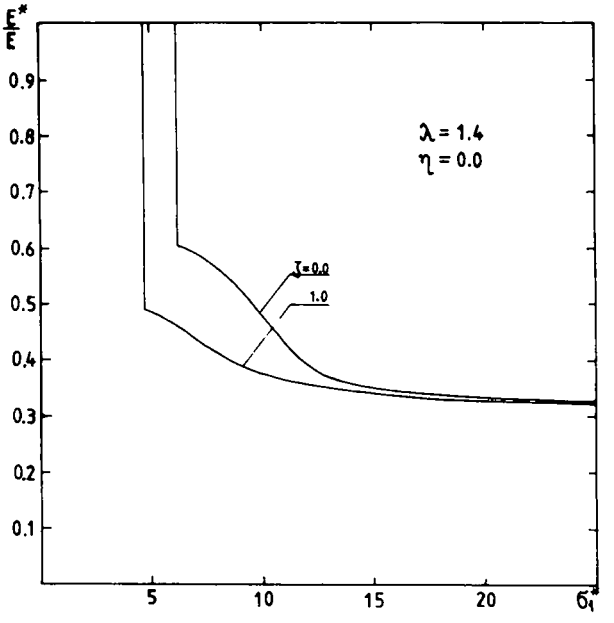

Fig. 14. Post-buckling stiffness E^*/E versus loading parameter σ_1^*.

Equation (29) when applied to a perfect plate produces a parabolic relationship between loading and maximum deflection.

Ref. 18 showed that the load-deflection curve of the perfect plate holds its parabolic character provided that the loading does not reach the far post-buckling range. The relationship between out of plan deflection and external loading for an imperfect plate takes the form

$$\sigma^* = \sigma^*_{cr}\left(1 - \frac{w_o^*}{w_t^*}\right) + G_1(w_t^{*2} - w_o^{*2}) \tag{30}$$

where

$$G_1^* = \frac{\sigma^* - \sigma_{cr}^*}{w_p^{*2}} \tag{31}$$

is the parameter of the parabola obtained from the theoretical results of the perfect plate.

Making use of the phenomenological and structural similarities an attempt was made to adopt the above-mentioned approach for the plates analysed in this paper.

The maximum deflection, $w^*_{p\max}$, obtained from theoretical calculations showed typical parabolic character (e.g. in Fig. 10). The coordinates x^*, y^* of $w^*_{p\max}$, however, were not fixed but have been changed due to changes of eigenvector parameters f_i^* with increasing

load of the plate. For comparison purposes, however, a point of fixed coordinates is needed so that its deflection could be compared with the experimental readings. Therefore, this point should be chosen in close vicinity to the place where the maximum deflection occurs. For the plate of aspect ratio $\lambda = 1{\cdot}4$, the point $x^* = 0{\cdot}7$, $y^* = 0{\cdot}5$ was chosen after a review of theoretical results.

The coefficient G_1 calculated using eqn (31) had to be averaged from the values obtained for a series of points of the curves σ_1^* versus w_p^*. For the typical case when compressional type of behaviour prevailed the discrepancies between the actual value of G_1 and the averaged value were of the order of 1%. For larger shear contributions, however, the curves σ_1^* versus w_p^* did not follow exactly the parabolic form and the G_1 coefficients were less consistent. Discrepancies for the latter case reached 5%.

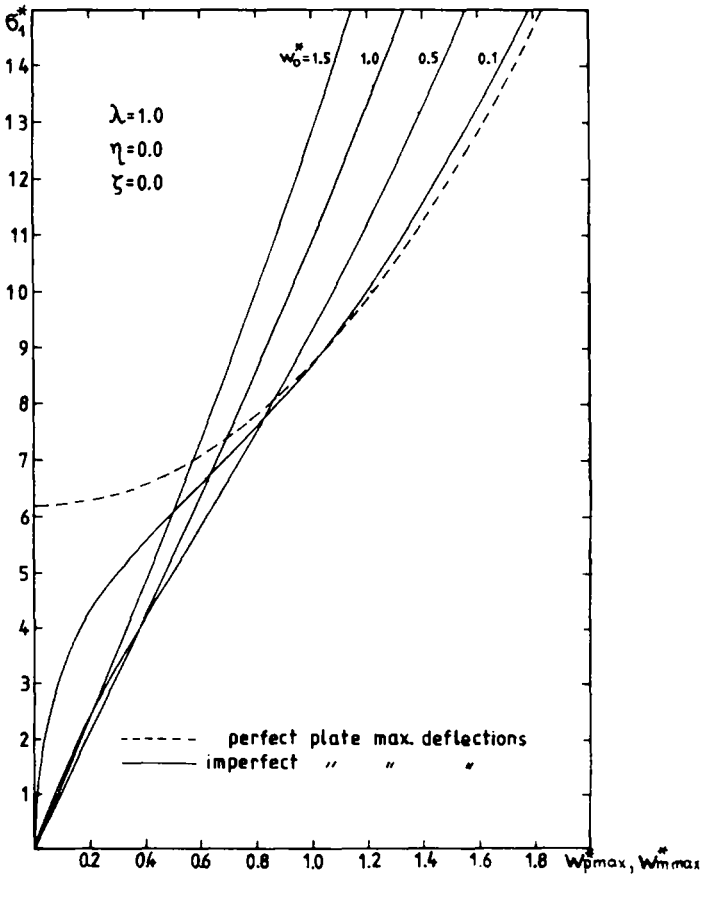

Fig. 15. Imperfect plate maximal deflection w^*_{mmax} versus loading parameter σ_1^*.

In Fig. 15, a typical example of the application of the simplified analysis to the imperfect plate is presented.

5 CONCLUSIONS

The energy method has been applied to analyse buckling and post-buckling of simply supported rectangular plates loaded by linearly varying compression and shear. The numerical analysis concerned a large range of plate aspect rations $\lambda(0{\cdot}6\text{–}1{\cdot}6)$, compression unequality factors $\eta(0{\cdot}0\text{–}1{\cdot}0)$ and shear stress coefficients $\zeta(0{\cdot}0\text{–}1{\cdot}0)$. The theoretical results showed that the post-buckling behaviour of the plate was greatly influenced by the magnitude of the shear contribution. For low shear coefficients compressional behaviour dominated, whereas for their higher values interaction type of behaviour was observed. The introduction of both direct shortening and shear distortion proved to be useful to depict the post-buckling stiffness of the plate. The maximum stress intensity obtained using the Huber-Hencky-Mises approach mainly occurred at one of the plate corners of the edge under higher compression. The eigenvector parameters f_i^* exhibited significant changes due to both the level of loading σ_1^* and the type of loading, which further resulted in a considerable reduction of the ratio of post-buckling to pre-buckling stiffness. The simplified approach has been successfully adopted to the analysis of imperfect plate behaviour.

REFERENCES

1. Bleich, F., *Buckling Strength of Metal Structures*. McGraw-Hill Book Co. Ltd, New York, 1952.
2. Timoshenko, S. P. & Gere, J. M., *Theory of Elastic Stability* (2nd edn). McGraw-Hill Book Co. Ltd, New York, 1961.
3. Volmir, A. S., *Ustoichiovost Deformiruyemych System*. Izdat. Nauka, Moscow, 1967 (in Russian).
4. Allen, H. G. & Bulson, P. S., *Background to Buckling*. McGraw-Hill Book Co. Ltd, London, UK, 1980.
5. Stein, M. & Neff, J., Buckling stress of simply supported rectangular flat plates in shear. *NACA*, Tech Note, No. 1222, 1947.
6. Porter, D. M., Rockey, K. C. & Evans, H. R., The collapse behaviour of plate girders loaded in shear. *The Structural Engineer*, **53**(8) (1975) 313.
7. Rhodes, J. & Harvey, J. M., Effects of eccentricity of load or compression on the buckling and post-buckling behaviour of flat plates. *Int. J. Mech. Sci.*, **13** (1971) 867–79.
8. Supple, W. J. & Wicks, P. J., *Post-Buckling Behaviour of Bi-axially Loaded*

Plates. Space Structure Research Centre, Department of Civil Engineering, University of Surrey, Guildford, UK, 1980.
9. Jakubowski, S., Analiza stanu zakrytycznego tarczy prostokątnej poddanej działaniu mimośrodowego sciskania. *Mechanika Teoretyczna i Stosowana*, **3/4**(20) (1982) 285–301 (in Polish).
10. Libove, C., Ferdman, S. & Reusch, J., Elastic buckling of a simply supported plate under a compressive stress. *NACA*, Tech Note No. 1891, 1949.
11. Królak, M., Stan krytyczny oraz analiza pracy w obszarze nadkrytycznym tarcz prostokątnych poddanych nierówomiernemu sciskaniu i scinaniu. *Archiwum Budowy Maszyn*, **XXV**(4) (1978) 663 (in Polish).
12. Protte, W., Zur Stegblechbeulung unter in Zwei Richtungen Linear Veranderlichen Normalspannungen und in Einer Richtung, Parabolish Veranderlichen Schubspannungen. *Tech. Mitt Krupp Forsch. Ber Band*, 32, Heft 1 (1974) (in German).
13. Harding, J. E., Hobbs, R. E., Neal, B. G. & Slatford, J., *Parametric Study on Plates Under Combined Direct and Shear In-Plane Loading*. Eng. Struc. Laboratories, Civil Eng. Dept., Imperial College, CESLIC Report BG 44, 1976.
14. Yamaki, N., Post-buckling behaviour of rectangular plates with small initial curvature loaded in edge compression. *J. Appl. Mech.*, **26**(1959) 407–14; **27** (1960) 335–42.
15. Stowell, E. Z. & Schwartz, E. B., Shear and uniform longitudinal compression. *NACA*, ARR, No. 3K13, 1943.
16. Rhodes, J. & Walker, A. C., *Developments in Thin-Walled Structures — 1*. Applied Science Publ., London, UK, 1982.
17. Williams, D. G. & Walker, A. C., Explicit solutions for the design of initially deformed plates subjected to compression. *Proc. Inst. Civ. Eng.*, **59** (1975) 763–87.
18. Rhodes, J. & Harvey, J. M., Examination of plate post-buckling behaviour. *Proc. ASCE — J. Eng. Mech. Div.*, **103** (1977) 461–76.
19. Zaraś, J., Buckling and post-buckling of rectangular plates under linearly varying compression and shear. PhD thesis, University of Strathclyde, UK, 1983.

APPENDIX 1: i, $\overline{m}_i$, $\overline{n}_i$, a_i

Indices i and related them integers $\overline{m}_i$, $\overline{n}_i$ together with the coefficients a_i of the stress function particular solution F_p given by eqn (7) are as follows:

i	$\overline{m}_i$	n_i	a_i	i	$\overline{m}_i$	n_i	a_i
1	1	0	$a_1 = (-f_1 f_2 + 9f_4 f_5)\frac{\lambda^2}{4}$	16	1	5	$a_{16} = \frac{36f_3 f_5\lambda^2}{(1+25\lambda^2)^2}$
2	2	0	$a_2 = f_1^2\frac{\lambda^2}{32}$	17	1	6	$a_{17} = \frac{225f_4 f_5\lambda^2}{4(1+36\lambda^2)^2}$
3	3	0	$a_3 = f_1 f_2\frac{\lambda^2}{36}$	18	2	4	$a_{18} = \frac{9f_1 f_5\lambda^2}{16(1+4\lambda^2)^2}$
4	4	0	$a_4 = (f_2^2 + 4f_3^2 + 9f_4^2)\frac{\lambda^2}{128}$	19	3	1	$a_{19} = \frac{4f_1 f_3\lambda^2}{(9+\lambda^2)^2}$
5	5	0	$a_5 = f_4 f_5\frac{9\lambda^2}{100}$	20	3	2	$a_{20} = \frac{(-f_1 f_2 + 25f_1 f_4)\lambda^2}{4(9+4\lambda^2)^2}$
6	6	0	$a_6 = f_3^2\frac{\lambda^2}{32}$	21	3	4	$a_{21} = -\frac{f_1 f_4\lambda^2}{4(9+16\lambda^2)^2}$
7	0	1	$a_7 = -(f_2 f_3 + f_3 f_4)\frac{1}{\lambda^2}$	22	4	1	$a_{22} = \frac{(9f_2 f_3 + 25f_3 f_4)\lambda^2}{(16+\lambda^2)^2}$
8	0	2	$a_8 = (f_1^2 + 4f_3^2 - 8f_2 f_4)\frac{1}{32\lambda^2}$	23	4	2	$a_{23} = \frac{(9f_1 f_5 + 16f_2 f_4)\lambda^2}{16(4+4\lambda^2)^2}$
9	9	3	$a_9 = f_2 f_3\frac{1}{9\lambda^2}$	24	4	3	$a_{24} = -\frac{f_2 f_3\lambda^2}{(16+9\lambda^2)^2}$
10	0	4	$a_{10} = (f_3^2 + 2f_2 f_4)\frac{1}{32\lambda^2}$	25	4	4	$a_{25} = -\frac{f_2 f_4\lambda^2}{64(1+\lambda^2)^2}$
11	0	5	$a_{11} = f_3 f_4\frac{1}{25\lambda^2}$	26	4	6	$a_{26} = -\frac{f_3 f_4\lambda^2}{(16+25\lambda^2)^2}$
12	0	6	$a_{12} = (4f_4^2 + 9f_5^2)\frac{1}{288\lambda^2}$	27	5	1	$a_{27} = \frac{36f_3 f_5\lambda^2}{(25+\lambda^2)^2}$
13	1	2	$a_{13} = \frac{(9f_1 f_3 - f_1 f_4 - 9f_2 f_5)\lambda^2}{4(1+4\lambda^2)^2}$	28	5	2	$a_{28} = \frac{81f_2 f_5\lambda^2}{4(25+\lambda^2)^2}$
14	1	3	$a_{14} = \frac{4f_1 f_3\lambda^2}{(1+9\lambda^2)^2}$	29	5	4	$a_{29} = -\frac{9f_2 f_5\lambda^2}{4(25+16\lambda^2)^2}$
15	1	4	$a_{15} = \frac{(25f_1 f_4 + 81f_2 f_5)\lambda^2}{4(1+16\lambda^2)^2}$	30	5	6	$a_{30} = -\frac{9f_4 f_5\lambda^2}{4(25+36\lambda^2)^2}$

APPENDIX 2

Displacement functions, $u(xy)$, $v(xy)$

The 'displacement field' of the middle plane of the plate consists of displacements $u(xy)$ and $v(xy)$.

$$u(xy) = \frac{\sigma_1}{E}\left[\frac{(2+\nu)(1-\eta)}{2}\left(\frac{y^2}{a} - \frac{y}{\lambda}\right) - \frac{(1-\eta)}{2a}x^2 - \eta x\right]$$

$$- \frac{\pi^2 x}{8a^2}(f_1^2 + 4f_2^2 + 4f_3^2 + 4f_4^2 + 9f_5^2) - 2\frac{\pi}{8a}\sum_{i=1}^{6} B_i \sin i\alpha x$$

$$+ \nu\frac{\lambda^2\pi}{4a}\sum_{i=1}^{6} C_i \sin i\alpha x + \frac{\pi}{a}\sum_{i=1}^{24} D_i \sin k_i\alpha x \cos l_i\beta y$$

$$+ \frac{\nu\pi\lambda^2}{a}\sum_{i=1}^{18} H_i \sin p_i\alpha x \cos q_i\beta y$$

$$v(xy) = \frac{\sigma_1}{E}\left\{\nu\frac{1-\eta}{a}xy + \left[2(1+\nu)\zeta - \nu\frac{1-\eta}{2\lambda}\right]x + \nu\eta y\right\}$$

$$- \frac{\pi^2\lambda^2}{8a^2}y(f_1^2 + f_2^2 + 4f_3^2 + 9f_4^2 + 9f_5^2) - \frac{\pi\lambda}{8a}\sum_{i=1}^{6} B_i' \sin i\beta y$$

$$+ \frac{\nu\lambda}{\lambda a}\sum_{i=1}^{6} C_i' \sin i\beta y - \frac{\pi\lambda}{a}\sum_{i=1}^{24} D_i' \cos k_i'\alpha x \sin l_i'\beta y$$

$$+ \frac{\nu\pi\lambda^3}{a}\sum_{i=1}^{18} H_i' \cos p_i'\alpha x \sin q_i'\beta y$$

The coefficients $B_i, C_i, D_i, H_i, B_i', C_i', D_i', H_i'$ and corresponding indices i, $k_i, l_i, p_i, q_i, k_i', l_i', p_i', q_i'$ are too lengthy to be presented in full extent. Their detailed presentation can be found in Ref. 19. It should be pointed out, however, that the coefficients B_i, C_i, B_i', C_i' are the functions of $(f_i\, f_j)$ whereas D_i, H_i, D_i', H_i' are expressed in terms of $(f_i\, f_j, \lambda)$.

Total plate shortening, u_o

$$u_o = \frac{\sigma_1}{2E}(1+\eta)\lambda b + \frac{\pi^2}{8\lambda b}(f_1^2 + 4f_2^2 + 4f_3^2 + 4f_4^2 + 9f_5^2)$$

Total plate distortion, v_o

$$v_o = \frac{\sigma_1}{E} 2\zeta(1+\eta)\lambda b + \frac{\pi}{b}\left[f_1 f_3 \frac{16(1093\lambda^4 + 234\lambda^2 - 27)}{3(1+9\lambda^2)^2(9+\lambda^2)^2}\right.$$

$$\left. + f_3 f_5 \frac{432(13021\lambda^4 + 1050\lambda^2 + 125)}{5(1+25\lambda^2)^2(25+\lambda^2)^2)}\right]$$

$$-\frac{\nu\pi\lambda^2}{b}\left[f_1 f_3 \frac{16(39\lambda^4 - 18\lambda^2 - 121)}{(1+9\lambda^2)^2(9+\lambda^2)^2} + f_3 f_5 \frac{432(105\lambda^4 + 50\lambda^2 + 521)}{(1+25\lambda^2)^2(25+\lambda^2)^2}\right]$$

APPENDIX 3: COEFFICIENTS OF ENERGY FUNCTION: W_{ij}, $W_{i(jkl)}$

The coefficients W_{ij} and $W_{i(jkl)}$ used in the energy function V in eqn (20) are

$$W_{15} = W_{51} = W_{23} = W_{32} = W_{24} = W_{42} = W_{34} = W_{43} = 0$$

$$W_{11} = \frac{\sigma_1 b^2}{E\pi^2}\frac{1+\eta}{2} - \frac{D}{Et}\left(\frac{1}{\lambda}+\lambda\right)^2; \quad W_{12} = W_{21} = -\frac{\sigma_1 b^2}{E\pi^2}\frac{40(1-\eta)}{9};$$

$$W_{13} = W_{31} = \frac{\sigma_1 b^2 \lambda}{E\pi^4}\zeta\frac{128}{9}$$

$$W_{22} = \frac{\sigma_1 b^2}{E\pi^2}2(1+\eta) - \frac{D}{Et}\left(\frac{4}{\lambda}+\lambda\right)^2; \quad W_{14} = W_{41} = -\frac{\sigma_1 b^2}{E\pi^4}4(1-\eta);$$

$$W_{35} = W_{53} = \frac{\sigma_1 b^2 \lambda}{E\pi^4}\zeta\frac{1152}{25}$$

$$W_{33} = \frac{\sigma_1 b^2}{E\pi^2}2(1+\eta) - \frac{D}{Et}\left(\frac{4}{\lambda}+4\lambda\right)^2;$$

$$W_{25} = W_{52} = -\frac{\sigma_1 b^2}{E\pi^4}\frac{36(1-\eta)}{25}$$

$$W_{44} = \frac{\sigma_1 b^2}{E\pi^2}2(1+\eta) - \frac{D}{Et}\left(\frac{4}{\lambda}+9\lambda\right)^2;$$

$$W_{45} = W_{54} = -\frac{\sigma_1 b^2}{E\pi^4}\frac{312(1-\eta)}{25}$$

$$W_{55} = \frac{\sigma_1 b^2}{E\pi^2}\frac{9(1+\eta)}{2} - \frac{D}{Et}\left(\frac{9}{\lambda}+9\lambda\right)^2$$

$$W_{1(111)} = -\frac{1+\lambda^4}{16\lambda^2}$$

$$W_{1(122)} = W_{2(112)} = \frac{1}{16}\left[-\frac{4(1+\lambda^4)}{\lambda^2} - \frac{81\lambda^2}{(1+4\lambda^2)^2} - \frac{\lambda^2}{(9+4\lambda^2)^2}\right]$$

$$W_{1(133)} = W_{3(113)} = 16\left[-\frac{\lambda^2}{(1+9\lambda^2)^2} - \frac{\lambda^2}{(9+\lambda^2)^2}\right]$$

$$W_{1(144)} = W_{4(114)}$$

$$= \frac{1}{16}\left[-\frac{\lambda^2}{(1+4\lambda^2)^2} - \frac{625\lambda^2}{(1+16\lambda^2)^2} - \frac{625\lambda^2}{(9+4\lambda^2)^2} - \frac{\lambda^2}{(9+16\lambda^2)^2}\right]$$

$$W_{1(155)} = W_{5(115)} = \frac{81}{16}\left[-\frac{\lambda^2}{(1+4\lambda^2)^2} - \frac{\lambda^2}{(4+\lambda^2)^2}\right]$$

$$W_{1(124)} = 2W_{4(112)} = 2W_{2(114)} = \frac{1}{8}\left[\frac{4}{\lambda^2} + \frac{9\lambda^2}{(1+4\lambda^2)^2} + \frac{25\lambda^2}{(9+4\lambda^2)^2}\right]$$

$$W_{1(245)} = W_{2(145)} = W_{4(125)} = W_{5(124)}$$

$$= \frac{9}{16}\left[-2\lambda^2 - \frac{\lambda^2}{(1+4\lambda^2)^2} - \frac{16\lambda^2}{(4+\lambda^2)^2} - \frac{225\lambda^2}{(1+16\lambda^2)^2}\right]$$

$$W_{1(225)} = \frac{1}{2}W_{2(125)} = W_{5(122)} = \frac{81}{16}\frac{\lambda^2}{(1+4\lambda^2)^2}$$

$$W_{2(222)} = -\frac{16+\lambda^4}{16\lambda^2}$$

$$W_{2(224)} = 3W_{4(222)} = \frac{3}{\lambda^2}$$

$$W_{2(233)} = W_{3(223)} = \left[-\frac{(16+\lambda^4)}{4\lambda^2} - \frac{81\lambda^2}{(16+\lambda^2)^2} - \frac{\lambda^2}{(16+9\lambda^2)^2}\right]$$

$$W_{2(244)} = W_{4(224)} = \frac{1}{16}\left[-\frac{64+9\lambda^4}{\lambda^2} - \frac{\lambda^2}{(1+\lambda^2)^2} - \frac{256\lambda^2}{(4+\lambda^2)^2}\right]$$

$$W_{2(255)} = W_{5(225)} = \frac{81}{16}\left[-\frac{\lambda^2}{(1+4\lambda^2)^2} - \frac{81\lambda^2}{(1+16\lambda^2)^2} - \frac{81\lambda^2}{(25+4\lambda^2)^2}\right.$$

$$\left. - \frac{\lambda^2}{(25+16\lambda^2)^2}\right]$$

$$W_{2(334)} = \frac{1}{2}W_{3(234)} = W_{4(233)} = 9\left[-\frac{1}{3\lambda^2} - \frac{25\lambda^2}{(16+\lambda^2)^2}\right]$$

$$W_{3(333)} = -\frac{1+\lambda^4}{\lambda^2}$$

$$W_{3(344)} = W_{4(334)} = \left[-\frac{(16+9\lambda^4)}{4\lambda^2} - \frac{625\lambda^2}{(16+\lambda^2)^2} - \frac{\lambda^2}{(16+25\lambda^2)^2}\right]$$

$$W_{3(355)} = W_{5(335)} = 1296\left[-\frac{\lambda^2}{(1+25\lambda^2)^2} - \frac{\lambda^2}{(25+\lambda^2)^2}\right]$$

$$W_{4(444)} = -\frac{16+81\lambda^4}{16\lambda^2}$$

$$W_{4(455)} = W_{5(445)} = \frac{1}{16}\left[-\frac{36+324\lambda^4}{\lambda^2} - \frac{(225\lambda)^2}{(1+36\lambda^2)^2} - \frac{81\lambda^2}{(25+36\lambda^2)^2}\right]$$

$$W_{5(555)} = -\frac{81}{16}\frac{(1+\lambda^4)}{\lambda^2}$$